https://doi.org/10.5194/egusphere-2026-1247
Preprint. Discussion started: 16 April 2026

Using artificial intelligence to monitor live fuel moisture content across France, based on a high-resolution land surface analysis

Yann Baehr[1], Pierre Vanderbecken[1], Bertrand Bonan[1], Catherine Robert[2], Mathieu Regimbeau[3], François Pimont[4], Kevyn Raynal[4], Xiangzhuo Liu[5], Remi Savazzi[7], Moncef Garouani[8], Josiane Mothe[9], Nemesio Rodriguez-Fernandez[6], Lionel Jarlan[6], and Jean-Christophe Calvet[1]

[1]Météo-France, CNRS, Univ. Toulouse, CNRM, Toulouse, France
[2]Météo-France, Direction des Opérations pour la Prévision, Coordination nationale feux de végétation, Toulouse, France
[3]Météo-France, Direction des Services Météorologiques, Division Agrométéorologie, Toulouse, France
[4]INRAE, URFM, Avignon, France
[5]INRAE, UMR1391 ISPA, Villenave d'Ornon, France
[7]ONF, pôle national DFCI, Direction territoriale Midi-Méditerranée, Aix-en-Provence, France
[6]CESBIO, University of Toulouse, IRD/CNRS/UPS/CNES, Toulouse, France
[8]IRIT, Univ. Toulouse Capitole, UMR5505 CNRS, Toulouse, France
[9]IRIT, UT2J, Univ. de Toulouse, UMR5505 CNRS, Toulouse, France

Correspondence: Jean-Christophe Calvet (jean-christophe.calvet@meteo.fr)

Abstract. Live Fuel Moisture Content (LFMC) is one of the most critical variables for understanding fire dynamics, particularly within forest environments. This study intends to develop a daily LFMC indicator to support operational fire danger management services in France. The product is based on in situ observations from the French National Forest Office and is generated using a lightweight expressive neural network model. The network has been designed to generalise well over time and space. It can be integrated directly into land surface models to enable real-time monitoring of vegetation's hydric status. The modelling framework combines outputs from a physically based land surface model and satellite-derived leaf area index (LAI) observations, providing high-resolution, spatially consistent estimates of land surface over France. To evaluate the model's generalisation capacity, we implemented complementary cross-validation strategies to test interannual robustness, spatial transferability, and to simulate an operational deployment scenario. Additionally, we performed a robustness analysis to quantify the sensitivity of predictions to training variability. The results demonstrate a strong ability to estimate the range and dynamics of LFMC across most of France. They also identify regions where additional in situ sampling or improved representation could reduce epistemic uncertainty and enhance the reliability of the model.

1 Introduction

In recent decades, forest fires have intensified worldwide, both in frequency and severity, under the combined effects of climate change and changes in land use and management (Pimont et al., 2023; Fernandez-Anez et al., 2021; Skinner et al., 2022; Jolly and Johnson, 2018). While wildfires have long been a natural part of many ecosystems, the risk posed by this natural danger is increasing, especially during periods of extreme weather such as severe droughts or heatwaves. Such periods tend to dry out vegetation, thereby increasing the risk of fire or even mega-fire events (McCaffrey, 2004). This impact is particularly pro-

https://doi.org/10.5194/egusphere-2026-1247
Preprint. Discussion started: 16 April 2026

nounced in temperate areas, including those across the Mediterranean basin. The interplay of elevated temperatures, protracted drought periods, and augmented fuel loads engenders conducive circumstances for the manifestation of extreme phenomena (Castel-Clavera et al., 2023; Dupuy et al., 2020; Bradstock, 2010; Kelley et al., 2019).

Temperate deciduous forests, mostly present in the Northern Hemisphere, are especially exposed to these risks (Loidi and Marcenò, 2022). Their structure and phenology, dominated by broadleaved species with high seasonal moisture dynamics, make them sensitive to changes in water availability and fuel moisture, both key drivers of fire behaviour (Jolly et al., 2014).

In this context, Live Fuel Moisture Content (LFMC) is often recognised as one of the most important variables for understanding fire behaviour, particularly in forest-dominated ecosystems (Forkel et al., 2023a; Chuvieco et al., 2004; Kang et al., 2023). The effects of LFMC on both the likelihood of ignition and the rate of fire propagation are well-documented, thus making it fundamental for the evaluation of fire danger. A substantial body of research has documented a robust correlation between LFMC and fire occurrence, particularly in Mediterranean regions (Chuvieco et al., 2023; Dimitrakopoulos et al., 2010; Luo et al., 2019), emphasising its importance as a key driver in the initiation and spread of fires (Pimont et al., 2019; Kelley et al., 2019; McNorton and Di Giuseppe, 2024).

Nevertheless, characterising the spatiotemporal pattern of LFMC remains challenging due to the scarcity and sparsity of field measurements, high interspecific variability, and heterogeneity in protocols depending on the organisation collecting the samples (Yebra et al., 2024; Viñuales et al., 2024). Consequently, operational fire danger rating systems either ignore or neglect the LFMC, or alternatively emphasise Dead Fuel Moisture Content (DFMC), which is more directly influenced by atmospheric conditions (McNorton and Di Giuseppe, 2024). However, mounting evidence suggests that minor fluctuations in LFMC, particularly during critical periods, may be sufficient to induce a substantial escalation in flammability in vegetation, even in cases where DFMC exhibits minimal variability (Awad et al., 2020; Viñuales et al., 2024; Finney et al., 2013; Chuvieco et al., 2005).

It is imperative to comprehend and model LFMC to accurately assess fire danger, ignition potential, and spread dynamics. Although several fire spread models incorporate LFMC as an input (Rothermel, 1972; Jolly et al., 2014; Pimont et al., 2019), the influence of LFMC on ignition probability is frequently overlooked or simplified in most fire danger rating systems (Anderson et al., 2015; Wang et al., 2017). The LFMC has been identified as a threshold variable, i.e. a variable that, when exceeded, results in vegetation becoming susceptible to ignition. It has been demonstrated that LFMC significantly modulates fire behaviour. Consequently, its effect may be underestimated in experimental field studies. This is frequently due to the limited spatial coverage, the uniform vegetation, and the substantial measurement uncertainties, which collectively fail to adequately represent the full range of LFMC conditions (Pimont et al., 2019).

Faced with these challenges, the increasing availability of remote sensing products, high-resolution land surface models, and the integration of machine learning methods now provide new opportunities to estimate LFMC at finer spatiotemporal scales (Jain et al., 2020; Rodriguez-Jiménez et al., 2023). Innovative approaches combining metadata and dynamic variables enable near-real-time predictions across large regions, which is essential to support operational fire risk systems in a context of accelerating environmental change (Shams Eddin et al., 2023; Fan et al., 2018; Preisler et al., 2004; Miller and Ager, 2012).

https://doi.org/10.5194/egusphere-2026-1247
Preprint. Discussion started: 16 April 2026

In particular, Benali et al. (2025) proposed a near-real-time operational LFMC product for Portugal at a national scale, which demonstrates the feasibility and relevance of integrating LFMC into fire danger decision-making systems.

This study aims to investigate the extent to which daily LFMC estimations could support fire management services in France. The resulting dataset will consist of an emulation of the output of a land surface model developed by Météo-France. By providing timely and spatially explicit estimates of vegetation flammability, this tool aims to improve both the speed and accuracy of decision-making processes. To achieve this, we design a deep learning model based on a neural network architecture, trained on in situ LFMC measurements and predictive soil variables derived from a land surface model. In Section 2, we present the data and methods, including the in situ sampling protocol, the post-processing of model inputs, the neural network architecture, and the validation strategies. Section 3 details the results and provides an analysis of the model's predictive performance and spatial outputs. Subsequently, Section 4 examines the implications of the methodology for operational fire management and delineates prospective advancements.

2 Materials and methods

2.1 In situ LFMC observations and data processing

The LFMC data used in this study comes from the Réseau Hydrique, an operational network established by the Office National des Forêts (ONF) in 1996 to improve fire danger assessment in the Mediterranean region of France (Martin-StPaul et al., 2018). This network is currently the only source of this variable across the territory. This network has gradually been extended to the south-west and then the north of France, with deployment in the south-west in 2023, then the northern half in 2024, reflecting a need to extend spatial coverage beyond the Mediterranean basin.

Each year, during the fire season (generally from June to September), samples are taken every week from around 110 sites and more than 40 plant species. The standard protocol involves sampling the apical and lateral shoots of living plants, representing a bunch weighing around 10 to 15 grams, collected between 11:00 and 13:00 UTC. These samples are immediately packed in numbered containers, sealed and refrigerated to prevent evaporation, then weighted before being dried at 60 °C for 24 hours (Martin-StPaul et al., 2018). Since 2023, the new sites (west and south-west) have used a desiccator balance. The old protocol is still used in the Mediterranean basin. The dry weight is then used to calculate the LFMC expressed in %, according to the standard formula:

$$\text{LFMC} = \frac{\text{mass}_{fresh} - \text{mass}_{dry}}{\text{mass}_{dry}} \times 100 \quad (1)$$

where mass_{fresh} and mass_{dry} represent the fresh and dry masses, respectively.

Sampling dates are systematically suspended if it has rained within the day preceding the scheduled date, in order to avoid a temporary overestimation of fuel moisture due to recent rainfall.

The processing of the raw data has been thoroughly revised to ensure its quality. This included conversion to a dry mass basis, identification of outliers (outside the normal biological range or strongly divergent from the rest of the day's measure-

https://doi.org/10.5194/egusphere-2026-1247
Preprint. Discussion started: 16 April 2026

ments), and estimation of robust indicators (weighted median) to better represent intra-site and intra-species variability. These treatments have been described in detail by Martin-StPaul et al. (2018) and allow better exploitation of the data for modelling.

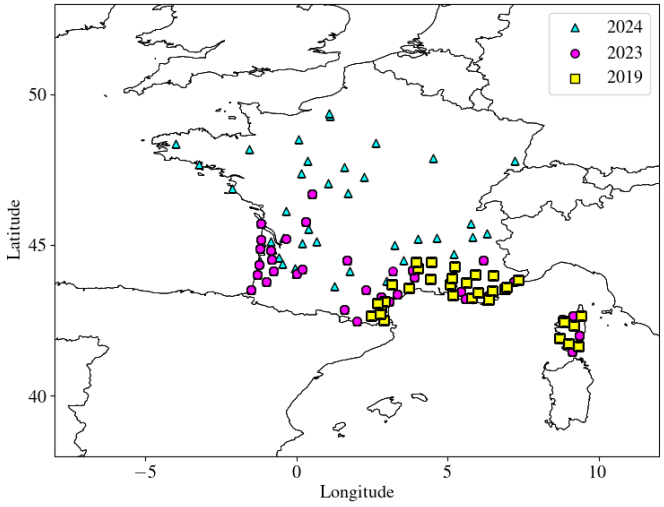

Figure 1. Overview of the study sites across France. The map shows the spatial distribution of field plots and the main regions analysed. This geographical diversity illustrates the contrasting climatic and ecological contexts used to assess LFMC dynamics. The historical sites of the 'Réseau Hydrique' are marked in yellow, the extended network of 2023 in magenta, and the 2024 network in cyan.

Figure 1 show a map of the sites of the Réseau Hydrique, which depicts both the oldest sites of the network and the most recent ones. A description of all the ONF's sites is included in the supplement in Table S1. An associated database, hosted online (Duché et al., 2017), contains all the raw and filtered data from 1996 to 2016, as well as the associated metadata.

For the rest of this work, for each site, LFMC measurements from different species collected on the same date were combined to compute an average shrub-level LFMC. As mentioned earlier, unlike the American protocol, the species are too varied to address LFMC on a species-by-species basis. Only dates with complete sampling for all species present were considered in sites with multi-species data. It should be noted that no information was available regarding the relative abundance of individual species or the height of the shrub layer, or the proportion of dead vegetation in the surrounding area.

Finally, while the standard LFMC formula used in Eq. 1 is commonly found in the scientific literature, an alternative definition is used by the ONF. This operational version, will be noted as LFMC_{fresh}, is computed as:

$$\text{LFMC}_{fresh} = \frac{\text{mass}_{fresh} - \text{mass}_{dry}}{\text{mass}_{fresh}} \times 100. \tag{2}$$

The two formulations are mathematically related and can be converted using the following equation:

$$\text{LFMC} = \frac{100}{\left(\frac{100}{\text{LFMC}_{fresh}} - 1\right)}. \tag{3}$$

https://doi.org/10.5194/egusphere-2026-1247
Preprint. Discussion started: 16 April 2026

As the modelling approach developed in this study was calibrated using observations from the ONF, the neural network was trained to predict LFMC_{fresh}. However, for consistency with the scientific studies, all reported LFMC values were converted to the usual LMFC_{dry} from LMFC_{fresh} using the above equation.

2.2 Predictor variables from land surface modelling

The land surface data used in this study are provided by the Application of Research to Operations at Mesoscale (Applications de la Recherche à l'Opérationnel à Méso-Échelle, AROME) driven Land Data Assimilation System (LDAS) system (LDAS-AROME), both developed and operated by Météo-France. This system combines the ISBA (Interaction Soil, Biosphere, and Atmosphere) land surface model with a Land Data Assimilation System (LDAS) to provide high-resolution, physically consistent estimates of surface variables over France.

ISBA (Noilhan and Planton, 1989) is a process-based model that simulates the exchanges of energy, water, and carbon between the land surface and the atmosphere. It explicitly represents soil moisture and temperature in multiple layers (Decharme et al., 2011), as well as vegetation dynamics, including plant phenology, biomass growth and senescence (Calvet et al., 1998). Specifically, the ISBA-A-gs option is used in this study (Calvet et al., 2004; Gibelin et al., 2006). ISBA is implemented within the SURFEX (Surface Externalisée) modelling platform, which allows for coupled or offline simulation of land and ocean surface variables and fluxes (Masson et al., 2013). The model accounts for sub-grid heterogeneity through a tiling approach, distinguishing between plant functional types (PFT), among them there is one dedicated to deciduous broadleaf forest, which will be used in the rest of the studies. Each PFT has its own specific water and energy budget.

Among the metadata predictors, the soil water field capacity (WFC) is of particular importance. WFC represents the maximum amount of water that a soil can retain against gravity after free drainage, and thus provides an upper bound for plant-available water. In ISBA, WFC is estimated from soil texture parameters (e.g. sand and clay fractions) provided in the physiographic database. It is important to note that, like the other metadata variables used in this study (e.g. slope, rugosity, soil texture and altitude), WFC is temporally constant but spatially heterogeneous. This ensures that the modelling framework takes into account local pedological and topographic conditions, while dynamic forcings from LDAS-AROME capture the temporal variability of soil and vegetation states.

Here, the ISBA land surface model in its aforementioned configuration is run in offline mode using atmospheric forecasts from the AROME-France numerical weather prediction system (Seity et al., 2011; Brousseau et al., 2016) that is run operationally by Météo-France. Daily forcing files with an hourly time step are produced using the first 12 hourly steps (T+1h to T+12h) of AROME-France forecasts issued at 00:00 UT and 12:00UTC. Variables used to force ISBA are: 2-m air temperature, 2-m specific humidity, 10-m wind speed, surface pressure, incoming shortwave and longwave radiation fluxes, and liquid and snow precipitation rates. Forecasts are then interpolated on a regular Cartesian grid with a spatial resolution of 1/40° over a domain centred on France. They are made available to the public through the Meteo-France BDAP database (Base de Données Analysées et Prévues, https://www.data.gouv.fr/datasets/donnees-pnt-retention-14-jours, in French).

To reduce the uncertainties of the simulations, ISBA is embedded in a sequential land data assimilation framework (LDAS) based on a Simplified Extended Kalman Filter (SEKF). This system assimilates remote sensing observations, such as satellite

https://doi.org/10.5194/egusphere-2026-1247
Preprint. Discussion started: 16 April 2026

products of Leaf Area Index (LAI), to constrain and correct the simulated vegetation states (Albergel et al., 2010; Barbu et al., 2014; Bonan et al., 2020; Rojas-Munoz et al., 2023). The assimilation generates an analysis, i.e., an improved estimate of the land surface conditions that incorporates both model predictions and observations. In contrast, open-loop simulations refer to model outputs without data assimilation and are often used for benchmarking or sensitivity analysis.

The outputs of LDAS-AROME, such as Soil Wetness Index (SWI), defined as soil moisture normalised between the wilting point and the field capacity, vegetation biomass, and surface temperature, provide a spatially and temporally consistent description of land surface conditions and are used as model inputs in this study.

In this study, LDAS-AROME outputs are used at a spatial resolution of approximately 2 km × 2 km. Within LDAS-AROME, satellite observations of LAI are assimilated every 10 days to improve the estimation of leaf biomass. The sequentially assimilated LAI data come from the global RT1 LAI product provided by the Copernicus Land Monitoring Service (CLMS). This product is derived from PROBA-V and Sentinel-3 satellite observations and is generated using a statistical approach based on a neural network algorithm. The latter was trained on two pre-existing LAI products to ensure robustness and consistency (Baret et al., 2013). The resulting LAI product is available globally at a 300 m × 300 m spatial resolution, with a temporal frequency of 10 days (European Environment Agency (EEA) / Copernicus Land Monitoring Service / European Commission's Joint Research Centre (2017), 2017).

2.3 Modelling using a neural network

Before adopting the architecture presented in this article, we evaluated several models based on recent methodological developments. First, we implemented a long short-term memory (LSTM) architecture inspired by the work of Rao et al. (2020), which produces monthly LFMC maps. We then adapted this architecture to suit the specifics of our problem and the characteristics of our daily LFMC maps. We retained the approach of mixing input parameters (Rao et al., 2020). We also assessed one-dimensional convolutional neural network architectures (Kiranyaz et al., 2021). However, due to technical constraints and the comparative performance of the candidate approaches, we decided against selecting any of these more complex methods, instead adopting the model described below.

We used a fully connected neural network to estimate the LFMC from a combination of dynamic (time-varying) and metadata (location-specific and day of the year) input features. This approach was chosen to ensure compatibility with the ISBA land surface model, as our objective is to eventually integrate the neural network into the ISBA modelling chain for operational applications. The network was implemented in Python using the Keras library, but limited to layers compatible with the *fnn* library coded in FORTRAN (Farchi, 2022) in order to be able to integrate it into the ISBA model in future developments. This library supports dense layers, dropout, and batch normalisation, enabling a lightweight model architecture.

Dense (fully connected) neural networks offer a flexible method for modelling nonlinear relationships between input and output variables. Although they lack explicit mechanisms for modelling temporal structure, as present in recurrent or attention-based architectures, recent work has shown that these models can still perform competitively on time series tasks (Das et al., 2024). Furthermore, the clear separation between dynamic and metadata inputs is a consequence of recent advances in location-

https://doi.org/10.5194/egusphere-2026-1247
Preprint. Discussion started: 16 April 2026

aware modelling (Shams Eddin et al., 2023), in which metadata variables are reintroduced at multiple levels of the model to ensure geographical specificity throughout the computation in stress monitoring.

The architecture is symmetrical and deep, with intermediate compressions followed by expansions. Figure 2 presents a schematic of the developed architecture. The model receives two inputs: the dynamic inputs (a vector of the variables extracted from the LDAS-AROME outputs) and the metadata inputs (extracted from the SURFEX V8 initialisation files, inspired by (Corchia, 2024)).

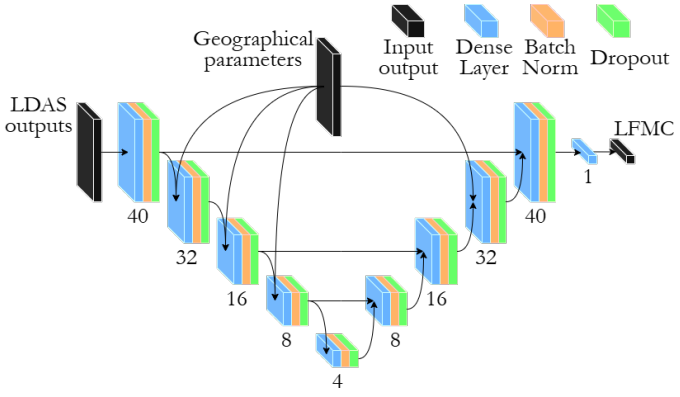

Figure 2. Schematic of the developed architecture composed of dense layers, dropout layers and batch-normalisation layers in order to be operationally implementable

The dynamic stream is first projected to a latent space of 4 dimensions via a dense layer, followed by ReLu activation, dropout (rate = 0.05), and batch normalisation. The hyperparameters are inspired by Rao et al. (2020). Metadata inputs are concatenated with the dynamic stream at four levels: after the first bottleneck (32 units), the second (16 units) and the one before the latent space, finally at the last bottleneck of 32 units symmetrically to the first. This design ensures that geographic information is present throughout the model, supporting robust generalisation across heterogeneous landscapes. That leads the model to adjust 7 000 parameters (two more experiments with more or fewer parameters have been tested and presented in Table S3 in the supplementary section). Additional experiments investigating the influence of the number of layers, the symmetry of the model, and the input injection strategy within the architecture have been conducted. Based on these results, we selected the configuration presented here.

The chosen optimiser was Adamax (Kingma and Ba, 2017), which is a variant of Adam based on the infinity norm, with a learning rate of 0.001. The loss function used was the mean-squared error (MSE). Early stopping based on the validation defined by the Nash–Sutcliffe model efficiency coefficient (see Section 2.6), with a patience of 50 epochs, was applied to avoid overfitting.

This neural architecture, designed to be lightweight yet expressive, enables direct integration into numerical land surface models for real-time vegetation stress monitoring.

https://doi.org/10.5194/egusphere-2026-1247
Preprint. Discussion started: 16 April 2026

2.4 Data partitioning and training strategy

Table 1 summarises the splitting process and the number of inputs in both the training and validation sets. The predictor's dataset spans from 2017 to 2024. To evaluate both temporal and spatial generalisation, we trained the model on data from 2017 to 2023 (2769 samples) and held out the entire year 2024 (916 samples across $\approx$ 40 newly instrumented sites) as an independent test set. Within the 2017–2023 period, we applied a year-wise random split of 70% of the samples for training and 30% for internal validation. This approach maximises the diversity of the training set while preserving unseen data for early-stopping and overfitting control.

Table 1. Sample counts per year for training, validation, and test sets. The year 2024 is used exclusively as an independent test.

Year	Month Start\End	Number of Sites	Train (70%)	Validation (30%)	Test	Total
2017	June\September	30	249	108	–	369
2018	June\September	33	192	83	–	283
2019	June\October	32	224	197	–	331
2020	June\September	35	245	106	–	367
2021	April\October	35	245	106	–	360
2022	April\October	47	289	124	–	425
2023	March\October	66	490	211	–	726
2017–2023	-	-	**1,934 (aggregated)**	**835 (aggregated)**	–	2,769
2024	June\September	93	–	–	916	916

After partitioning, we performed a data-driven feature selection using the `Optuna` package (Akiba et al., 2019), a framework for hyperparameter optimisation based on Bayesian sampling and pruning strategies to avoid redundancy in inputs. Optuna constructs a surrogate model of the objective function and iteratively explores the search space using a Tree-structured Parzen Estimator. In our case, the objective was to maximise the Nash–Sutcliffe Efficiency (NSE) on the validation set.

We ran 15,000 optimisation trials, each evaluating a different subset of predictors drawn from the state variables of the land-surface model as well as mixed variables (mixed between dynamics inputs and metadata inputs), such as presented in Rao et al. (2020), by training a lightweight neural network and recording the validation NSE. To accelerate convergence, unpromising trials were early-pruned using `Optuna`'s built-in median rule. The ten most frequently selected features across high-performing trials were retained as the most informative predictors (Table 2).

To represent the seasonal cycle, we encoded the day of the year (DOY) using a trigonometric transformation. Instead of the standard sin/cos encoding bounded in [–1,1], we applied a rescaling to match the order of magnitude of the metadata predictors. Specifically, we defined:

$$\texttt{DOY\_sin} = 365.25(1 + \sin(2\pi\,\mathrm{DOY}/365.25)/4) \tag{4}$$

$$\texttt{DOY\_cos} = 365.25(1 + \cos(2\pi\,\mathrm{DOY}/365.25)/4) \tag{5}$$

https://doi.org/10.5194/egusphere-2026-1247
Preprint. Discussion started: 16 April 2026

Table 2. Ten predictors selected by Optuna after 15000 trials (optimised on NSE). Variables originate from the ISBA-A-gs model.

Variable	Description	Type	Unit	Shapley scores
LAI/WFC	LAI normalized by field capacity (WFC)	Dynamic	–	0.04
SWI	Soil Water Index at layer 3 (4–10 cm depth)	Dynamic	–	0.02
Fuel	Leaf + structural above-ground biomass	Dynamic	kgDMm$^-$2	0.02
DOY_sin	$365.25(1+\sin(2\pi\,\mathrm{DOY}/365.25)/4)$	Metadata	–	0.01
Altitude	Elevation above sea level	Metadata	m a.s.l	0.01
Rugosity	Terrain rugosity (standard deviation of altitude)	Metadata	m	0.01
DOY_cos	$365.25(1+\cos(2\pi\,\mathrm{DOY}/365.25)/4)$	Metadata	–	0
Leaf Biomass	Biomass of leaf compartment (proportional to LAI)	Dynamic	kgDMm$^-$2	0
SAND	Sand fraction in the soil layer	Metadata	%	0
Slope	Mean micro-relief slope within the grid cell	Metadata	degrees	0

This ensures that the encoded variables have a comparable numerical scale with physiographic covariates (e.g. elevation, soil texture), facilitating the optimisation during training.

These selected features were then used to train the neural network with early stopping (patience $= 50$ epochs on validation NSE), yielding the final model evaluated in Section 3.1. The supplementary section contains Figures S1 and S2, which spatially illustrate those features for the 13th of August 2022 and 2023. The selection of predictors aligns with the vegetation type under consideration in this study. Shrubland ecosystems are distinguished by the relatively shallow nature of their root systems, which facilitates the utilisation of the SWI from the upper soil layers. Moreover, the incorporation of LAI is physically significant due to its robust correlation with vegetation density and transpiration processes, in addition to its pertinence to the ONF field measurements. The utilisation of the normalised LAI will be discussed in Section 4.6.

2.5 Evaluation and Cross-Validation

First, we evaluate the model on the 2024 dataset. We compute the site-averaged value of LFMC site by site (by using Equation 6, where s represents a specific site and t a specific sampling date), which allows us to see how the model manages to perform spatially. And finally, the Equation 7 expresses the LFMC anomalies relative to each site mean, enabling an evaluation of the model's ability to reproduce temporal dynamics, where s represents a specific site and t a specific sampling date.

$$\overline{LFMC}(s) = \left(\sum_{t=1}^{n} LFMC(s,t)\right)/n \tag{6}$$

$$LFMC'(s) = LFMC(s,t) - \overline{LFMC}(s) \tag{7}$$

To evaluate the generalisation capacity of the model across both space and time, we implemented three complementary cross-validation strategies:

https://doi.org/10.5194/egusphere-2026-1247
Preprint. Discussion started: 16 April 2026

First, the Forward-Chaining (FC), in this scenario, the model is trained using past years only, mimicking a real-world forecasting setting. For example, to predict LFMC in 2020, the model is trained on data from 2017 to 2019. This strategy reflects a strict chronological training setup, preventing data leakage and providing insight into the model's performance in operational forecasting conditions.

In the Leave-One-Year-Out (LOYO) scenario, the model is trained on all available years except one, which is used for testing. For example, to evaluate performance in 2020, the model is trained on data from 2017, 2018, 2019, 2021, 2022, 2023, and 2024. This setup allows us to assess the model's ability to generalise to unseen temporal conditions, including interannual variability in climate and vegetation.

Finally, the Leave-One-Site-Out (LOSO) model is trained on all sites except three, which are randomly selected to ensure a comprehensive survey of the sites. This approach is adopted to avoid sites with only one measurement, thereby ensuring the attainment of more reliable statistics. The model is then subjected to testing to ascertain its spatial generalisation capacity, i.e. its ability to predict LFMC at locations not encountered during the training process.

Each validation strategy targets a specific dimension of model robustness and helps characterise its strengths and limitations across temporal, spatial, and predictive contexts.

In addition to cross-validation and large-scale application over France and neighbouring regions, we conducted an analysis of model robustness to assess the sensitivity of LFMC predictions to the training process. To this end, we performed an ensemble of 500 independent training runs of the model architecture, each with different random weight initialisations and data shuffling. The training was carried out on the full dataset, using identical hyperparameters and input configurations for all runs.

For each model instance, LFMC was predicted over the AROME grid for a fixed evaluation date (13 August 2022 and 2023), and the results were aggregated across the runs. We then computed the standard deviation of the predicted LFMC values for each spatial location, yielding a map of model prediction variability.

This standard deviation can be interpreted as a measure of the model's epistemic uncertainty; that is, uncertainty arising from limited knowledge acquired during the training process. Regions with higher standard deviation values suggest locations where the model exhibits less consistency across runs, indicating a greater sensitivity to initial conditions or an insufficient representation in the training data.

The final step of the evaluation consisted in estimating LFMC over the full-time period available from the AROME atmospheric forcing, from 1 January 2017 to present. This long-term simulation allows us to assess the ability of the model to reproduce both interannual variability and seasonal dynamics of LFMC. We focus the comparison on the time series of selected study sites where in situ measurements are available.

2.6 Metrics used to evaluate the model

The evaluation of the model was done by using four metrics, each capturing a different aspect of the predictive skill, where y is the observed value, $\hat{y}$ the estimated value, $\bar{y}$ the averaged observations, $\bar{\hat{y}}$ the averaged estimations and N the number of element:

https://doi.org/10.5194/egusphere-2026-1247
Preprint. Discussion started: 16 April 2026

Root Mean Square Error (RMSE) measures the average magnitude of the prediction errors, penalising large deviations more severely. It is expressed in percentages and is defined as:

$$\mathrm{RMSE} = \sqrt{\frac{1}{N}\sum_{i=1}^{N}(y_i - \hat{y}_i)^2} \tag{8}$$

Pearson correlation coefficient (R) represents the correlation between predicted and observed values. Captures the ability to follow dynamics. This metric ranges from -1 (perfect negative correlation) to $+1$ (perfect positive correlation). It is defined as:

$$R_{y\hat{y}} = \frac{\sum_{i=1}^{N}(y_i - \bar{y})(\hat{y}_i - \bar{\hat{y}})}{\sqrt{\sum_{i=1}^{N}(y_i - \bar{y})}\sqrt{\sum_{i=1}^{N}(\hat{y}_i - \bar{\hat{y}})}} \tag{9}$$

Nash-Sutcliffe Efficiency (NSE) is commonly used in hydrological modelling (Nash and Sutcliffe, 1970). The NSE evaluates how well the predicted time series matches the observations, relative to the mean of the observations. It is defined as:

$$\mathrm{NSE} = 1 - \frac{\sum_{i=1}^{N}(y_i - \hat{y}_i)^2}{\sum_{i=1}^{N}(y_i - \bar{y})^2} \tag{10}$$

An NSE of 1 indicates perfect prediction, 0 indicates the model is as good as using the mean of observations, and values < 0 indicate poor performance.

Kling-Gupta Efficiency (KGE, Gupta and Kling (2011)) combines correlation, bias, and variability errors into a single metric. It addresses some known limitations of the NSE. The KGE was preferred as a complementary metric to NSE and RMSE, as it provides a balanced assessment of correlation, bias, and variability, and helps disentangle the respective contributions of these error sources. It is defined as:

$$\mathrm{KGE} = 1 - \sqrt{(R-1)^2 + (\beta - 1)^2 + (\gamma - 1)^2} \tag{11}$$

where, R is the Pearson correlation coefficient, $\beta = \bar{\hat{y}}/\bar{y}$ is the bias ratio, $\gamma = \mathrm{CV}_{\hat{y}}/\mathrm{CV}_y$ is the variability ratio, and CV is the coefficient of variation.

These metrics were computed at various aggregation levels (e.g. per year, per site, and globally), depending on the validation strategy. All metrics were implemented using standard definitions in Python (e.g. `scipy`, `numpy`, or `hydroeval`).

https://doi.org/10.5194/egusphere-2026-1247
Preprint. Discussion started: 16 April 2026

3 Results

3.1 Model evaluation in 2024: temporal and spatial extrapolation

We evaluated the final model, which was trained using data from 2017 to 2023 and assessed using an independent dataset from 2024 comprising 916 samples collected from new locations. Figure 3(a) illustrates the joint density plot comparing predicted and observed LFMC for the year 2024. Figure 3(b) displays the model performance based on the averaged LFMC values across different sites. Additionally, Fig. 3(c) depicts the temporal variations, highlighting the model's ability to detect temporal changes.

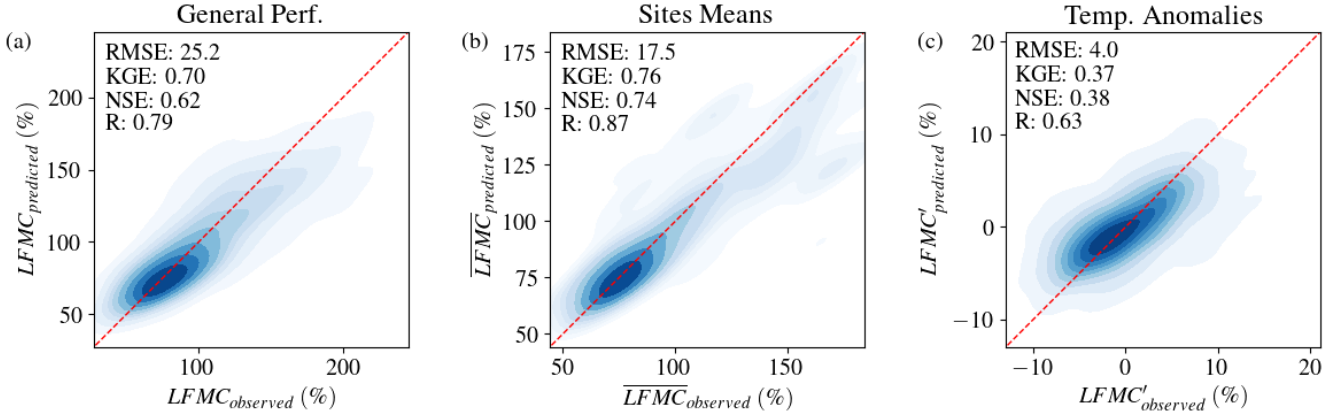

Figure 3. Scatter plots (joint density) of LFMC predictions versus observations for the 2024 test set. (a) Overall performance based on 916 estimated values, (b) site-averaged LFMC over the 92 monitored sites, and (c) temporal anomalies computed from the 916 test values. The intensity of the circle represents the density of the points.

The model accurately represents both the seasonal fluctuations and the range of observed LFMC values. While it successfully encapsulates the spatial mean of LFMC across various sites, it does not adequately capture the full amplitude range, despite the reduced bias and high correlation.

The quantitative evaluation confirms this: on the independent 2024 dataset, the model achieves competitive scores across all metrics, comparable to those obtained through cross-validation. Additional scores are reported in the supplementary section. The first set of scores in Table S2 is based on the historical Réseau Hydrique across the Mediterranean Sea, and the second set is based on the fresh mass (Fig. S3 shows the scatter plots of the mass$_{fresh}$).

These results indicate a good overall generalisation to sites and climatic regimes not seen during training, while also revealing a non-trivial variability across validation folds. Table 3 summarises the mean and standard deviation of the performance metrics (RMSE, NSE, KGE, and Pearson's R) for each cross-validation strategy, along with the scores on the independent 2024 test set. Although the average performance is similar across all schemes, the wider dispersion observed in the LOSO and FC setups

https://doi.org/10.5194/egusphere-2026-1247
Preprint. Discussion started: 16 April 2026

Table 3. Comparison of model performance across cross-validation schemes on an independent test set derived from both the analysis and the open-loop simulations and model performance across cross-validation schemes. Metrics are averaged and computed on the full 2024 test set. The best score values are highlighted in bold.

LFMC evaluation experiment	RMSE %	KGE	NSE	Pearson R	Number of points
Neural network trained with analysis applied to the analysis					
`Overall performance`	**25.2**	**0.70**	**0.62**	**0.79**	916
`Site-averaged`	**17.5**	0.76	**0.74**	**0.87**	92
`Temporal anomalies`	**4.0**	0.37	**0.38**	**0.63**	916
FC	22.7 ± 5.5	0.52 ± 0.14	0.08 ± 0.49	0.59 ± 0.12	see Table 1
LOYO	18.5 ± 3.5	0.57 ± 0.10	0.41 ± 0.16	0.67 ± 0.10	see Table 1
LOSO	20.3 ± 8.5	0.58 ± 0.24	0.40 ± 1.03	0.72 ± 0.20	see Table S1
Neural network trained with open-loop applied to the open-loop					
`Overall performance`	28.0	0.64	0.53	0.75	916
`Site-averaged`	21.0	0.71	0.63	0.81	92
`Temporal anomalies`	**4.0**	0.35	**0.38**	0.62	916
Neural network trained with analysis applied to the open-loop					
`Overall performance`	25.5	0.72	0.61	0.78	916
`Site-averaged`	17.8	**0.78**	0.73	0.86	92
`Temporal anomalies`	4.1	**0.45**	0.35	0.62	916

indicates that a small subset of sites or years accounts for a disproportionate share of the total error. Nevertheless, every strategy maintains the LFMC seasonal pattern, which supports the spatial transferability of the proposed approach.

Fig 4 (a) illustrates the FC scenario, where we train sequentially on increasing subsets of years.

For the FC, the skills score tends to increase with the number of years of training. However, this trend is interrupted twice: once for the 2020 prediction and again for the 2022 prediction. The drop in NSE for the FC in 2020 is due to the first substantial expansion of observation sites beyond the Mediterranean basin, which occurred in 2020. With only sites in the Mediterranean as part of the training database from 2017 to 2019, the neural network failed to accurately estimate those new sites. Once these sites were included in the training, the NSE of the FC improved again. The second noticeable drop occurs in 2022 for both FC and LOYO. The extremely dry summer of 2022 shows the importance of having representative extreme events in the training database for robust LFMC prediction.

In the Fig. 4 (b), omitting the year 2022 from the training set causes the NSE to drop markedly, from approximately 0.55 to 0.0, reflecting the atypical drought conditions experienced that year. The other years exhibit relatively stable performance (NSE $\approx$ 0.45–0.55 in LOYO configuration), indicating that the model handles interannual variability well except when a particularly extreme year is excluded.

To illustrate the LOSO scenario and how the scores can evolve, we select three specific sites, presented in the Fig. 5.

https://doi.org/10.5194/egusphere-2026-1247
Preprint. Discussion started: 16 April 2026

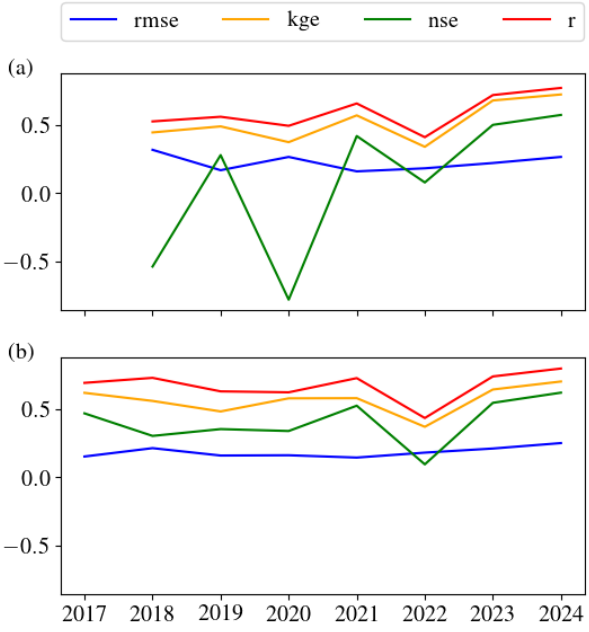

Figure 4. Evolution of the scores under (a) Forward-Chaining (FC) and (b) Leave-One-Year-Out (LOYO) validation schemes.

'Les Adrechs' is the first site presented in Fig. 5(a), which is a site close to the Mediterranean Sea, an area well studied in space and time. Even if the site is omitted, the neural network managed to obtain a correlation score close to 0.80. In Fig. 5(b), 'Forêt de la Coubre' is a newly added site located near the Atlantic Ocean, situated in an area that is spatially well covered in 2023 and 2024. However, its correlation score appears to decrease to 0.72 when compared with the preceding, well-temporally-covered site. Moreover, Fig. 5(c) corresponds to 'La Chapelle-Moulière', an isolated area in central France that is poorly represented both spatially and temporally. Although the range is fairly good, the correlation is low, close to 0. This suggests the model can estimate LFMC dynamics reasonably well across the area, but still needs more information for robust generalisation.

3.2 Spatial mapping of predictions

We applied the trained model, with 2024 as the evaluation dataset, pixel-wise over the AROME grid for a fixed date in 2022 and 2023. Figure 6 shows the resulting LFMC prediction maps. The selected date, August 13, corresponds to the day with the lowest average LFMC across France during the summer of 2022, based on a temporal analysis of daily LFMC values. Figure S4 in the supplementary document illustrates the method used to select this specific day.

Figure 6 reveals that the spatial patterns of predicted LFMC on 13 August 2022 and 2023 closely follow the expected climatological gradients and land-cover characteristics. Higher moisture levels are found in mountainous, forested regions

https://doi.org/10.5194/egusphere-2026-1247
Preprint. Discussion started: 16 April 2026

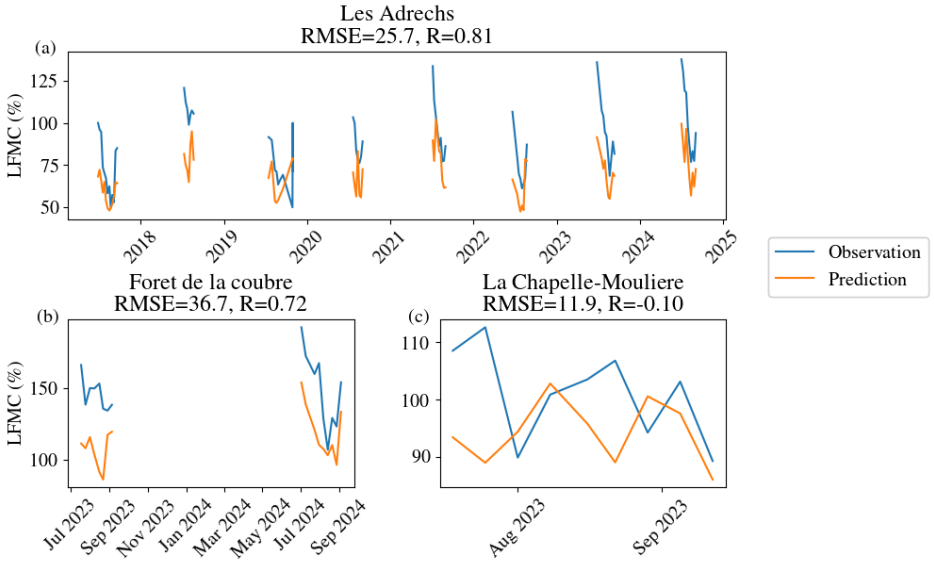

Figure 5. Illustration of spatial generalization under the Leave-One-Site-Out (LOSO) validation. Comparison between observed and predicted LFMC at three representative sites: (a) Les Adrechs (Mediterranean, well-sampled, from 2017 to 2024), (b) Forêt de la Coubre (Atlantic, moderately represented, from 2023 to 2024), and (c) La Chapelle-Moulière (isolated site in 2023). All the estimated values shown are paired with the observed values during the summer.

(e.g. the Massif Central, the Vosges, and the Alps) and coastal areas (e.g. lhe Landes areas) in both years, while lower LFMC values prevail in Mediterranean areas and the northern plains.

Figure 6 (c) presents the pixel-wise difference $\Delta\mathrm{LFMC} = \mathrm{LFMC}_{2023} - \mathrm{LFMC}_{2022}$ for 13 August. Rather than following a simple south–north gradient, the anomaly map reveals that the western, north-western, northern, and even north-eastern regions experienced the largest moisture deficits in 2022 compared with summer 2023, with differences up to 20%. In contrast, the Mediterranean basin, already characterised by low LFMC in both years, shows only moderate anomalies. This spatial pattern shows that the summer 2022 drought was particularly severe and anomalous in regions that are usually more temperate, highlighting its unusual geographic extent and intensity.

3.3 Prediction uncertainty: ensemble standard deviation

To assess epistemic uncertainty, that is, the sensitivity of the model to randomly drawn initialisations and data limitations, we generated an ensemble of 500 independently trained models. Each model was applied across the AROME grid for 13 August 2022, and we computed the standard deviation of the predictions at each grid point. Figure 7 displays the resulting maps.

Overall, the variability remains remarkably low across most of France, with ensemble standard deviations typically ranging between 1.0% and 7.5% LFMC. This suggests strong robustness of the model's predictions in well-covered areas of the domain.

https://doi.org/10.5194/egusphere-2026-1247
Preprint. Discussion started: 16 April 2026

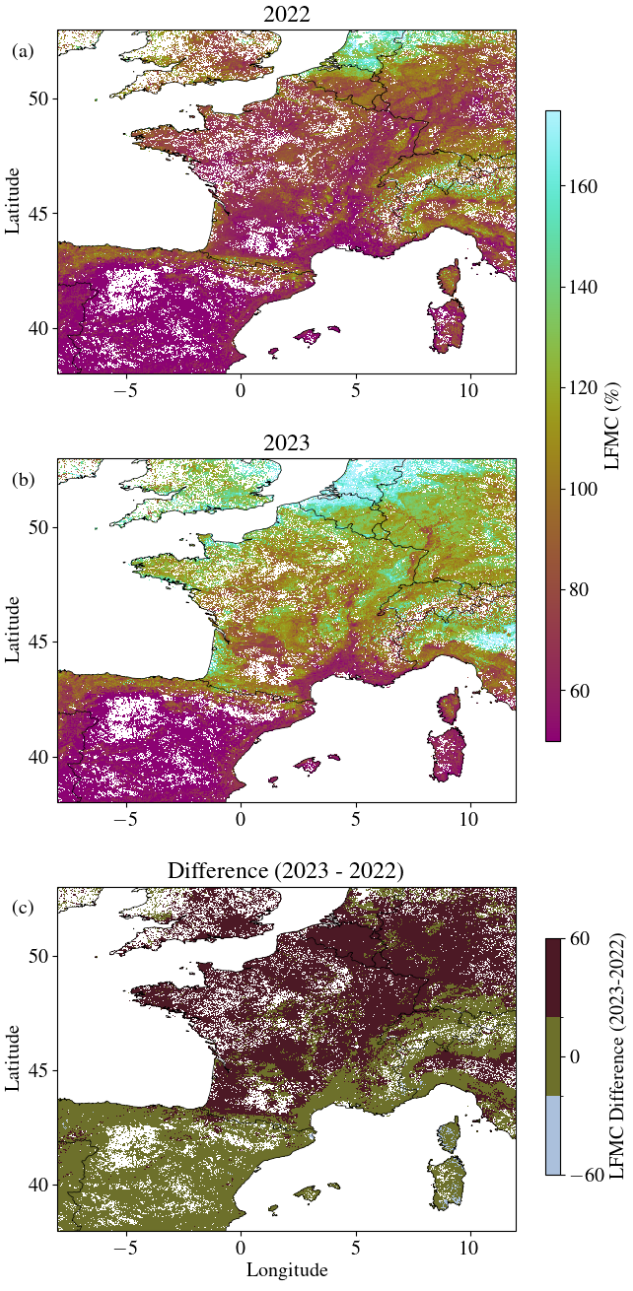

Figure 6. Spatial distribution of predicted LFMC on 13 August 2022 (a) and 2023 (b) over the AROME grid. LFMC anomaly map (c) highlighting the 2022 summer drought ($LFMC_{2023} - LFMC_{2022}$) on 13 August. The red shading corresponds to positive values, i.e. locations where LFMC in 2023 exceeds that of 2022, indicating that 2022 was comparatively drier. Conversely, grey areas (negative values) denote spots where 2022 remained wetter than 2023.

https://doi.org/10.5194/egusphere-2026-1247
Preprint. Discussion started: 16 April 2026

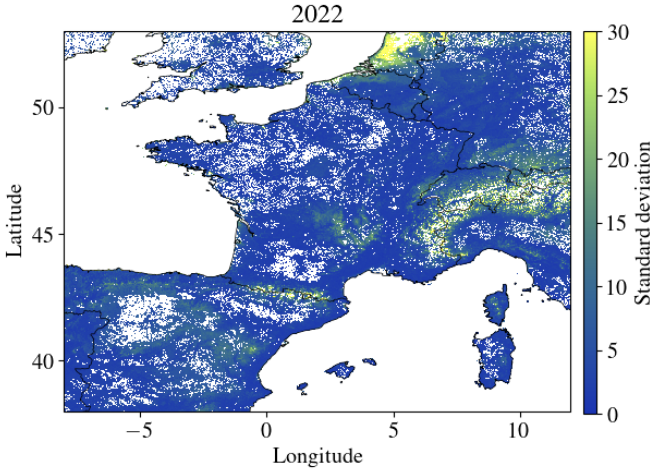

Figure 7. Ensemble-based standard deviation of LFMC predictions for 13 August 2022, over 500 runs. Higher values highlight areas of greater model uncertainty.

Other experiments have been made on different dates. However, the variation in standard deviation from one date to another is very low, so only one date is presented in this paper.

Higher uncertainty values appear primarily along coastlines and in mountainous areas, including the Alps, the Pyrenees, and the Massif Central. These zones often correspond to grid cells where the fraction of temperate deciduous forests is underrepresented, making predictions more sensitive to small changes in training conditions.

Outside the mountain chains, the model also shows elevated uncertainty over the Netherlands and parts of Belgium, areas that lie completely outside the spatial extent of the ONF observation network. This is consistent with a lack of training data in these zones, and further illustrates the model's sensitivity to extrapolation beyond its calibration domain. Furthermore, forests in these regions may exhibit structural and compositional characteristics that differ from those represented in the training dataset, including a higher proportion of coniferous and younger forests. Such differences can impact vegetation structural attributes and plant water-use strategies.

Figure 8 displays the temporal evolution of modelled (orange line) and observed (blue markers) LFMC at the Les Adrechs site for the period 2017–2025.

Observations collected between 2017 and 2023 were used to calibrate and cross-validate the model; they therefore provide an in-sample benchmark. During this period, the model accurately reproduced both the seasonal cycle (spring peaks and late-summer troughs) and the interannual variability, with only minor amplitude biases.

Of particular interest is the extrapolation beyond the calibration window. For the fully unseen year 2024, the simulated trajectory remains consistent with the expected seasonal pattern and closely tracks the limited in situ measurements available to date, suggesting good generalisation skills.

https://doi.org/10.5194/egusphere-2026-1247
Preprint. Discussion started: 16 April 2026

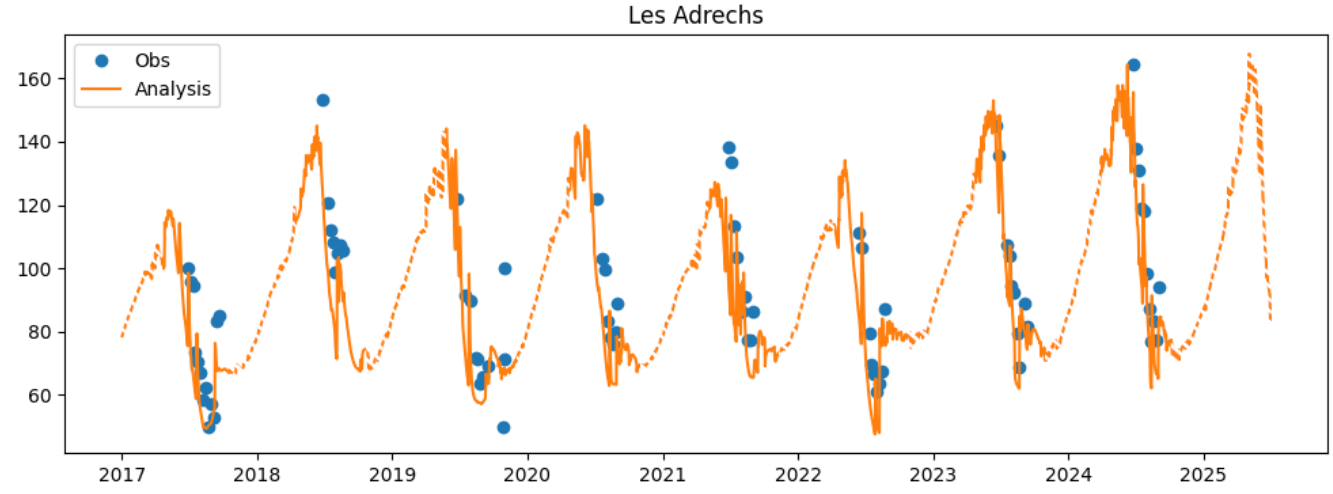

Figure 8. Time series of observed and modelled LFMC at Les Adrechs (2017–2025). The blue dots correspond to the measurements from the Réseau Hydrique, while the orange line shows the estimated evolution of LFMC over the years. The dashed lines indicate temporal intervals for which no empirical data are available to constrain or calibrate the model, implying that the model output in these regions corresponds to an extrapolation over an extended time period.

4 Discussion

4.1 To what extent does the model demonstrate robustness and operational potential?

The complementary experiments presented in Sections 3.1 to 3.3 highlight several key aspects of model robustness. First, interannual evaluations confirm that generalisation is maintained across most years. However, predictive performance improves markedly when the training dataset encompasses both a broad spectrum of geographic conditions (as in 2020) and extreme anomalies (as in 2022). This highlights the need for a wider training database for even more robust prediction. Second, the spatial analyses show that the model consistently uses metadata predictors (such as elevation, soil texture, and micro-relief) alongside dynamic inputs to reproduce physiographically coherent moisture distributions. Finally, the forward-looking simulations suggest that the model can already anticipate seasonal dynamics at unseen sites, pointing to a strong potential for operational deployment once continuous observational datasets become available.

Overall, these findings attest to the ensemble's robustness across most of France, while simultaneously delineating spatially explicit regions where additional in situ sampling or improved patch representation could reduce epistemic uncertainty and thereby increase model reliability.

A key limitation must nonetheless be acknowledged: the model was trained exclusively on field observations collected during the fire season (typically June to September). Consequently, its ability to capture vegetation dynamics during colder months has not yet been evaluated, and its current operational applicability is restricted to the warm-season period, when fire danger is most acute.

https://doi.org/10.5194/egusphere-2026-1247
Preprint. Discussion started: 16 April 2026

4.2 Is simulated LFMC consistent with real fire occurrence?

In order to test whether the simulated LFMC values are consistent with the actual ignition events, we retrieved all the recorded fire outbreaks that occurred between June and September 2022 in France main land. We then analysed the temporal evolution of the canton-averaged LFMC values around these events (see Fig. 9). A map of French cantons, which are government-defined administrative units with surface areas ranging from approximately 4 km^2 in urban settings to about 1,000 km^2 in rural regions, is provided in the Supplementary Material (see Fig. S5).

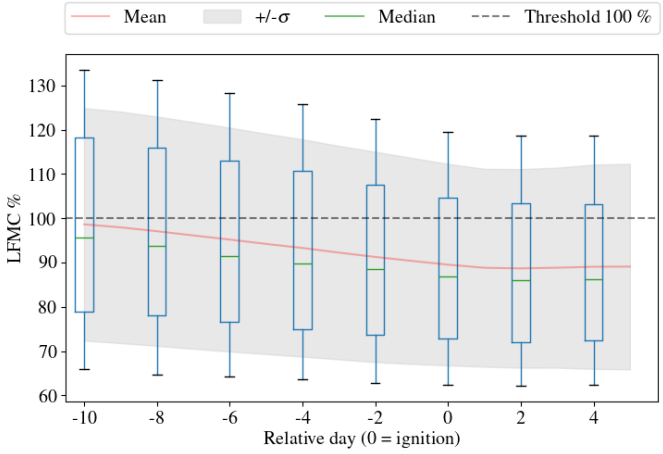

Figure 9. Temporal evolution of canton-averaged LFMC around ignition events in France (June–September 2022).

The analysis shows a monotonic decline in LFMC during the ten days preceding ignition, with mean values converging towards 90% on the ignition day. Both the mean and the median fall well below 100%, which is close to the moisture of extinction (ME) threshold reported in the literature for shrublands (around 105%; Chuvieco et al. (2004)). This supports the interpretation that simulated LFMC captures vegetation flammability conditions at the landscape scale.

Figure 9 also highlights that ignition is not associated with short-term anomalies, but rather with a sustained decline in LFMC leading up to the event. This is consistent with experimental and modelling studies showing that fuel moisture content strongly influences ignition probability and fire spread once values drop below 100% (Luo et al., 2019). Our results, therefore, suggest that simulated LFMC dynamics are in good agreement with observed fire occurrence and that operational thresholds for fire danger could be defined in terms of ME ranges identified in the literature.

Finally, these results suggest the potential for using simulated LFMC products in fire risk assessments, particularly in the context of fire likelihood (Castel-Clavera et al., 2025). Integrating LFMC dynamics into these platforms could therefore enhance warning capabilities by offering meaningful thresholds related to vegetation flammability, complementing existing meteorological indices for fire risk assessment.

https://doi.org/10.5194/egusphere-2026-1247
Preprint. Discussion started: 16 April 2026

4.3 Can the model guide the deployment of new measurement stations?

Beyond site-level validation, our framework can also highlight regions where additional field monitoring would most improve model robustness. To this end, we combined (i) the spatial distribution of model uncertainty and (ii) the distance to existing ONF sites to derive a composite "interest score" for each grid cell. A K-means clustering was then applied to classify the French territory into zones of low and high priority for new station deployment (see Supplementary Material Section 8 for details).

As shown in Fig. 10, northern and north-eastern France, as well as cross-border regions, systematically emerge as underrepresented areas where epistemic uncertainty remains high.

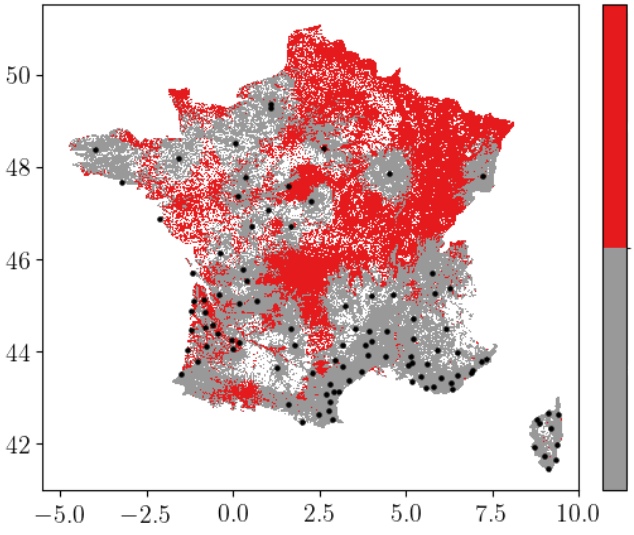

Figure 10. Prioritisation map for new LFMC monitoring sites in France. The classification combines model uncertainty and distance to existing ONF sites, with clusters identified using K-means. Black dots show the current ONF network. The areas highlighted in red on the map indicate regions where further observations are required to improve spatial coverage.

These zones appear critical for expanding the LFMC monitoring network, since they currently lack proximal training sites. In contrast, southeastern France and Corsica are already well covered by existing stations, and thus contribute less to reducing overall uncertainty.

From an operational standpoint, this prioritisation exercise provides a practical decision-support tool. It helps identify locations where the establishment of new stations would maximally reduce uncertainty and increase the representativeness of the training dataset. Nevertheless, one limitation remains the vegetation specificity of the current network: most ONF sites monitor shrubs, while forests with closed canopy or grass-dominated systems may display distinct drought responses. Diversifying the network to capture this ecological heterogeneity would further improve model generalisation.

https://doi.org/10.5194/egusphere-2026-1247
Preprint. Discussion started: 16 April 2026

4.4 Is the integration of new satellite observations feasible and beneficial?

Given the increasing availability of high-resolution Earth observation data (e.g., from Sentinel-2, MODIS, or VIIRS), an important avenue for future work is the integration of new satellite observations, in addition to CLMS LAI. Could remote sensing observations, such as land surface temperature, microwave radiances, or active fire detections, enhance the spatio-temporal representativity of the model and support near-real-time applications?

Integrating new satellite-based observations into the modelling framework opens promising avenues for both research and operations. Three main strategies can be envisioned:

(1) Comparative analysis with remotely sensed proxies, such as surface moisture indices derived from Sentinel-2 (e.g., NDWI, NDMI) or microwave vegetation optical depth (VOD) products (Moesinger et al., 2020; Forkel et al., 2023b), could help benchmark and refine the model's outputs without altering its architecture.

(2) Direct integration of satellite images, while conceptually attractive, presents operational challenges, particularly in terms of data acquisition frequency, cloud coverage except for low microwave frequencies, and processing constraints. In academic contexts, however, exploring alternative architectures (e.g., convolutional or hybrid neural networks) could allow the spatial structure of satellite imagery to be effectively exploited.

(3) Assimilation-inspired approaches, akin to what is done in the LDAS system (e.g., with LAI), offer a practical compromise. Satellite-derived variables could be used to periodically recalibrate or constrain the model's outputs without disrupting its real-time operability. Moreover, as shown by Corchia et al. (2023), the assimilation of radar backscatter observations via a neural-network observation operator can further improve the constraint on LAI in an LDAS framework. This hybrid approach may bridge the gap between operational simplicity and enhanced spatial representativity.

The integration of remote sensing data provides several opportunities. Comparative benchmarks with indices such as NDWI or microwave VOD could help validate spatial patterns without changing the model architecture. Although more ambitious approaches, such as the direct ingestion of imagery through convolutional layers, remain technically feasible, they raise questions regarding operational costs, sensitivity to cloud cover and processing latency. A pragmatic compromise is the periodic recalibration of model outputs using satellite proxies (assimilation-inspired approach), which may enhance spatial representativity while preserving near-real-time operability. Future work combining our framework with EO-based LFMC products (e.g. Yebra et al. (2024); Benali et al. (2025)) could bridge the gap between local and continental scales, as well as align with the methodological framework and variable selection adopted by Liu et al. (2026) for local LFMC estimation across the Mediterranean basin.

4.5 What is the impact of LAI assimilation on model performance?

In this section, we examine the impact of LAI assimilation on the model's performance. First, we compare the model trained on the analysis and evaluated on the analysis, then the model trained on the open loop and evaluated on the open loop, and finally the model trained on the analysis and evaluated on the open loop. As shown in Fig.11, the assimilation of LAI into ISBA has a clear influence on the simulated LFMC.

https://doi.org/10.5194/egusphere-2026-1247
Preprint. Discussion started: 16 April 2026

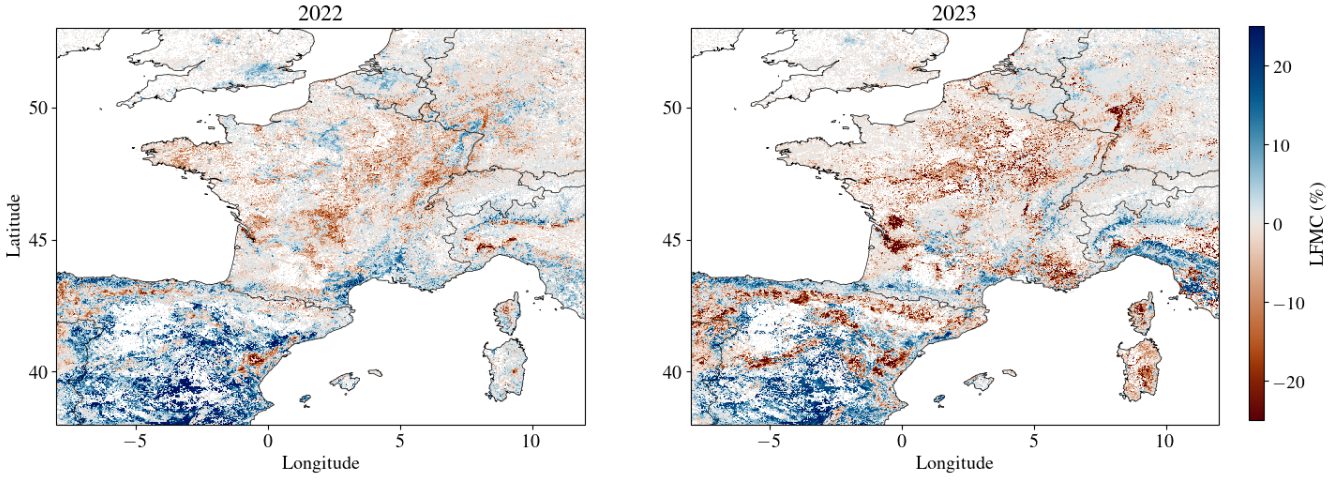

Figure 11. Relative difference in LFMC between analysis and open-loop simulations for 2022 and 2023, 13th of August. Positive values indicate higher LFMC after LAI assimilation, while negative values indicate lower LFMC.

Since LFMC estimates rely on ISBA prognostic variables, constraining vegetation dynamics with observed LAI improves the consistency of the surface model and propagates to the LFMC predictions. The comparison between open-loop and analysis configurations shows that the impact is highly heterogeneous across space and time. In 2022, when drought conditions prevailed in Southern Europe, the assimilation process generally led to an increase in LFMC estimates in regions suffering from water stress, such as the Iberian Peninsula and southern France, while it decreased the values in central France and the northeast. In 2023, the impact of assimilation showed a slight increase across the entire territory.

These results underline that the benefit of LAI assimilation is context-dependent: the correction of vegetation dynamics is particularly valuable under extreme conditions, either by compensating for model underestimations during droughts or by constraining excessive LFMC in wetter years. Overall, LAI assimilation enhances the realism of vegetation–water interactions in ISBA, leading to more reliable LFMC simulations and a better representation of interannual variability.

In addition, Table 3 illustrates the application of the model, trained using the analysis fields, to the 2024 dataset extracted from the open-loop simulation in comparison with the previously presented scores obtained from the analysis. We observe that scores have deteriorated for those trained using the open-loop scenario, which highlights the necessity of continuing to use the analysed product for training purposes. Conversely, the model's robustness is demonstrated by its ability to produce consistent scores when used with open-loop data. This suggests that, firstly, metadata plays an important role in estimating the LFMC and, secondly, the loss function used enables the model to estimate average values, but struggles to represent extremes regardless of the experiment.

https://doi.org/10.5194/egusphere-2026-1247
Preprint. Discussion started: 16 April 2026

4.6 How can the LAI/WFC predictor be interpreted ?

Among the predictors retained by the optimisation process, the variable LAI/WFC showed a particularly strong influence on model performance. Although this ratio is not a standard variable in the literature, its importance can be interpreted from a biophysical standpoint.

The normalisation of LAI by the soil water field capacity (WFC) implicitly couples two complementary aspects of vegetation functioning: the seasonal evolution of canopy density and the local capacity of the soil to store and supply water. In areas with low WFC, even moderate increases in LAI can lead to strong soil–plant competition for water, amplifying drought stress and, consequently, reducing LFMC. Conversely, in regions with higher WFC, vegetation growth (higher LAI) is less constrained by water availability.

By introducing this ratio, the model is thus encouraged to learn the interaction between vegetation phenology and soil water-holding properties, rather than treating them as independent drivers. This is also consistent with the fact that different soil types tend to host different plant functional types, whose phenological dynamics and water-use strategies are shaped by the underlying soil properties. This likely explains its high weight in the feature selection process and its strong contribution to predictive skill, especially under conditions of rapid vegetation development or during dry-down phases.

In practice, this result highlights the importance of jointly considering vegetation dynamics and soil hydraulic capacity when modelling live fuel moisture content, as both jointly modulate the balance between transpiration demand and available soil water.

4.7 Evaluation of input feature importance

A feature neutralisation approach was implemented to quantify the contribution of each predictor to model performance. After training the model as described above, analysis was conducted using the full set of observations available from 2017 to 2024, including those used for training. In each experiment, one predictor was neutralised at a time across the entire dataset. This involved replacing it with its spatial mean value computed over the domain while setting the day of year predictor to 0, while other predictors remained unchanged. The trained model was then applied to these modified datasets, and the resulting predictions were compared to the corresponding observations. To quantify the information loss, four metrics were used: the KGE, Pearson's correlation coefficient R, the bias, and the SDD (Standard Deviation of Differences). All metrics were normalised for comparison, and the signs of the KGE and R were inverted so that larger values corresponded to greater performance degradation. Further details on the influence of DOY are available in the supplements (see Table S4 for the scores obtained in the experiments. Figures S6 and S7 show the scatter plots).

The resulting performance scores are summarised in Fig. 12, where the surface area of each polygon represents the degree of performance loss when the corresponding variable is neutralised. A larger area indicates a stronger influence of that variable on model accuracy.

https://doi.org/10.5194/egusphere-2026-1247
Preprint. Discussion started: 16 April 2026

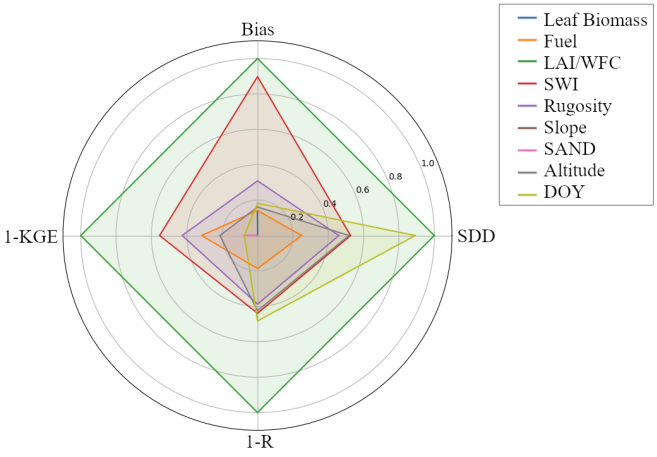

Figure 12. Variable neutralisation experiment. The colored regions indicate the influence of each variable when neutralised; smaller areas correspond to a lower impact on the model's decision.

The analysis reveals that the LAI/WFC ratio exerts the largest impact on predictions, confirming its role as a primary control on vegetation water status. In contrast, metadata such as topographic slope or sand fraction show only marginal effects when individually neutralised, although they still contribute to spatial generalisation.

To complement this perturbation-based approach, we computed `SHAP` (SHapley Additive exPlanations) scores from the trained neural network ensemble. The `SHAP` feature ranking (Table 2, column **Shapley scores**) shows consistent importance patterns with the neutralisation experiment, particularly highlighting LAI/WFC, biomass, and soil water indices as the dominant predictors of LFMC variability. This agreement between independent methods reinforces the interpretability and robustness of the modelling framework.

5 Conclusions

This study presents a lightweight but effective neural network model for monitoring Live Fuel Moisture Content (LFMC) across France, trained on in situ measurements and land surface model outputs. The framework demonstrates strong generalisation capacity across years and sites, accurately reproducing both seasonal dynamics and spatial gradients. Through dedicated cross-validation and ensemble experiments, we showed that the model maintains robust predictive skill even under atypical climatic anomalies, such as the 2022 drought.

By combining static physiographic predictors (as well as the day of the year) with dynamic variables, the model yields spatially coherent LFMC fields, consistent with known land use patterns. Importantly, our analysis highlights that performance benefits from including both diverse geographic conditions (e.g., the extended part of the Réseau Hydrique, including the West and North regions of France) and extreme anomalies (e.g., 2022) in the training pool. Operational potential is underscored

https://doi.org/10.5194/egusphere-2026-1247
Preprint. Discussion started: 16 April 2026

by the model's ability to extrapolate to newly instrumented sites in 2024, while uncertainty maps to guide the deployment of future monitoring stations.

Nevertheless, some limitations remain. The model has so far been trained on warm-season observations (May–September). Future efforts that incorporate measurements collected outside the fire season will extend its applicability throughout the year. In particular, adding winter observations will enable the model to more fully capture and represent cold-season vegetation dynamics. In addition, regions beyond the current monitoring network show higher epistemic uncertainty, calling for expanded sampling and integration of satellite proxies. Future work will explore hybrid strategies that combine neural predictions with remote sensing products, with the aim of scaling the approach to continental domains and supporting near-real-time fire danger monitoring.

Code availability. The analysis was carried out with Python codes that can be made available upon request. SURFEX can be downloaded freely at http://www.umr-cnrm.fr/surfex/data/OPEN-SURFEX/open_surfex_v8_1_20210914.tar.gz (CNRM, 2016). It is provided under a CECILL-C license (French equivalent to the LGPL license).

Data availability. This publication has been prepared using the European Union's Copernicus Land Monitoring Service information; https://doi.org/10.2909/219fdc9f-616b-444b-a495-198f527b4722. All the data needed to trace the figures is available at the following address: https://doi.org/10.5281/zenodo.18850161.

Author contributions. YB and JCC designed the experiments. YB performed the investigation, did the formal analysis, and wrote the paper. BB processed the LDAS-AROME data set. All co-authors participated in the interpretation of the results and the revision of the paper.

Competing interests. No competing interests are present

Acknowledgements. The PhD work of Yann Baehr was supported by the Occitanie Region as part of the Earth Observation and Territories in Transition Key Challenge (O3T) and by Météo-France. This research received funding from European Union Horizon Europe through the CORSO project (grant agreement 101082194) and the GREENEO project (grant agreement 101183071). Views and opinions expressed are those of the authors only and do not necessarily reflect those of the European Union or the Commission. Neither the European Union nor the granting authority can be held responsible for them. The authors sincerely thank the colleagues, Marius Cadier, Bernard Chapnik, and Laura Pavan at Météo-France for their assistance in the operational implementation of the model during summer 2025. We also acknowledge the colleagues, Valentin Durinck, Elodie Beaumont and Jean-Luc Kicin at the ONF for their support in the deployment and integration of the system into operational activities.

https://doi.org/10.5194/egusphere-2026-1247
Preprint. Discussion started: 16 April 2026

References

Akiba, T., Sano, S., Yanase, T., Ohta, T., and Koyama, M.: Optuna: A Next-generation Hyperparameter Optimization Framework, in: Proceedings of the 25th ACM SIGKDD International Conference on Knowledge Discovery and Data Mining, https://optuna.org/, 2019.

Albergel, C., Calvet, J., Gibelin, A., Lafont, S., Roujean, J., Berne, C., Traullé, O., and Fritz, N.: Observed and modelled ecosystem respiration and gross primary production of a grassland in southwestern France, Biogeosciences, 7, https://doi.org/10.5194/bg-7-1657-2010, 2010.

Anderson, K., Simpson, B., Hall, R. J., Englefield, P., Gartrell, M., and Metsaranta, J. M.: Integrating forest fuels and land cover data for improved estimation of fuel consumption and carbon emissions from boreal fires, International Journal of Wildland Fire, 24, 665–679, https://doi.org/10.1071/WF14142, 2015.

Awad, C., Morvan, D., Rossi, J., Marcelli, T., Chatelon, F., Morandini, F., and Balbi, J.: Fuel moisture content threshold leading to fire extinction under marginal conditions, Fire Safety Journal, 118, 103 226, https://doi.org/10.1016/j.firesaf.2020.103226, 2020.

Barbu, A. L., Calvet, J., Mahfouf, J.-F., and Lafont, S.: Integrating ASCAT surface soil moisture and GEOV1 leaf area index into the SURFEX modelling platform : a land data assimilation application over France, Hydrology and Earth System Sciences, 18, https://doi.org/10.5194/hess-18-173-2014, 2014.

Baret, F., Weiss, M., Lacaze, R., Camacho, F., Makhmara, H., Pacholcyzk, P., and Smets, B.: GEOV1: LAI and FAPAR Essential Climate Variables and FCOVER Global Time Series Capitalizing over Existing Products. Part1: Principles of Development and Production., Remote Sensing of Environment, 137, 299 – 309, https://doi.org/10.1016/j.rse.2012.12.027, 2013.

Benali, A., Baldassarre, G., Loureiro, C., Briquemont, F., Fernandes, P. M., Rossa, C., and Figueira, R.: A Near-Real-Time Operational Live Fuel Moisture Content Product to Support Decision-Making at the National Level, Fire, 8, 178, https://doi.org/10.3390/fire8050178, 2025.

Bonan, B., Albergel, C., Zheng, Y., Barbu, A., Fairbairn, D., Munier, S., and Calvet, J.: An ensemble square root filter for the joint assimilation of surface soil moisture and leaf area index within the Land Data Assimilation System LDAS-Monde : application over the Euro-Mediterranean region, Hydrology and Earth System Sciences, 24, https://doi.org/10.5194/hess-24-325-2020, 2020.

Bradstock, R.: A biogeographic model of fire regimes in Australia: current and future implications, Global Ecology and Biogeography, 19, 145–158, https://doi.org/10.1111/j.1466-8238.2009.00512.x, 2010.

Brousseau, P., Seity, Y., Ricard, D., and Léger, J.: Improvement of the forecast of convective activity from the AROME-France system, Quarterly Journal of the Royal Meteorological Society, 142, 2231–2243, https://doi.org/10.1002/qj.2822, 2016.

Calvet, J., Noilhan, N., Roujean, J., Bessemoulin, P., Cabelguenne, M., Olioso, A., and J.P., W.: An interactive vegetation SVAT model tested against data from six contrasting sites, Agricultural and Forest Meteorology, 92, https://doi.org/10.1016/S0168-1923(98)00091-4, 1998.

Calvet, J.-C., Rivalland, V., Picon-Cochard, C., and Guehl, J.-M.: Modelling forest transpiration and CO2 fluxes—Response to soil moisture stress, Agricultural and Forest Meteorology, 124, 143 – 156, https://doi.org/10.1016/j.agrformet.2004.01.007, 2004.

Castel-Clavera, J., Pimont, F., Opitz, T., Ruffault, J., Barbero, R., Allard, D., and Dupuy, J.-L.: A comparative analysis of fire-weather indices for enhanced fire activity prediction with probabilistic approaches, Agricultural and Forest Meteorology, 361, 110 315, https://doi.org/https://doi.org/10.1016/j.agrformet.2024.110315, 2025.

Castel-Clavera, J. et al.: Disentangling the factors of spatio-temporal patterns of wildfire activity in south-eastern France, International Journal of Wildland Fire, 32, 15–28, https://doi.org/10.1071/WF22086, 2023.

Chuvieco, E., Aguado, I., and Dimitrakopoulos, A.: Conversion of fuel moisture content values to ignition potential for integrated fire danger assessment, Canadian Journal of Forest Research, 34, 2284–2293, https://doi.org/10.1139/X04-101, 2004.

https://doi.org/10.5194/egusphere-2026-1247
Preprint. Discussion started: 16 April 2026

Chuvieco, E., Camia, A., Bianchini, G., Margaleff, T., Koutsias, N., and Martinez, J.: Using remote sensing and GIS for global assessment of fire danger, In Conference Proceedings: Proceedings of the 22nd International Cartographic Conference. Global Congresos, https://publications.jrc.ec.europa.eu/repository/handle/JRC31405, 2005.

Chuvieco, E., Yebra, M., Martino, S., Thonicke, K., Gómez-Giménez, M., San-Miguel, J., Oom, D., Velea, R., Mouillot, F., Molina, J., and et al.: Towards an Integrated Approach to Wildfire Risk Assessment: When, Where, What and How May the Landscapes Burn, Fire, 5, 215, https://doi.org/10.3390/fire6050215, 2023.

Corchia, T.: Contribution of machine learning to the integration of satellite observations into a global model of the soil-plant system, Theses, Université de Toulouse, https://theses.hal.science/tel-04848876, 2024.

Corchia, T., Bonan, B., Rodríguez-Fernández, N., Colas, G., and Calvet, J.-C.: Assimilation of ASCAT Radar Backscatter Coefficients over Southwestern France, Remote Sensing, 15, https://doi.org/10.3390/rs15174258, 2023.

Das, A., Kong, W., Leach, A., Mathur, S., Sen, R., and Yu, R.: Long-term Forecasting with TiDE: Time-series Dense Encoder, https://arxiv.org/abs/2304.08424, 2024.

Decharme, B., Boone, A., Delire, C., and Noilhan, J.: Local Evaluation of the Interaction between Soil Biosphere Atmosphere Soil Multilayer Diffusion Scheme Using Four Pedotransfer Functions, Journal of Geophysical Research: Atmospheres, 116, https://doi.org/10.1029/2011JD016002, 2011.

Dimitrakopoulos, A., Mitsopoulos, I., and Gatoulas, K.: Assessing ignition probability and moisture of extinction in a Mediterranean grass fuel, International Journal of Wildland Fire, 19, 29–34, https://doi.org/10.1071/WF08124, 2010.

Duché, Y., Savazzi, R., Toutchkov, M., and Cabanne, E.: Multisite and Multispecies Live Fuel Moisture Content (LFMC) Series in the French Mediterranean Since 1996, https://doi.org/10.5281/zenodo.162978, 2017.

Dupuy, J., Fargeon, H., Martin-StPaul, N., and et al.: Climate change impact on future wildfire danger and activity in southern Europe: a review, Annals of Forest Science, 77, 35, https://doi.org/10.1007/s13595-020-00933-5, 2020.

European Environment Agency (EEA) / Copernicus Land Monitoring Service / European Commission's Joint Research Centre: Leaf Area Index 2014–present (raster 300 m), global, 10-daily – version 1, EEA Geospatial Data Catalogue, https://doi.org/10.2909/219fdc9f-616b-444b-a495-198f527b4722, 2017.

Fan, L., Wigneron, J., Xiao, Q., Al-Yaari, A., Wen, J., Martin-StPaul, N., Dupuy, J., Pimont, F., Al Bitar, A., Fernandez-Moran, R., and Kerr, Y.: Evaluation of microwave remote sensing for monitoring live fuel moisture content in the Mediterranean region, Remote Sensing of Environment, 205, 210–223, https://doi.org/10.1016/j.rse.2017.11.020, 2018.

Farchi, A.: https://doi.org/10.5281/zenodo.7245291., 2022.

Fernandez-Anez, N., Krasovskiy, A., Müller, M., and et al.: Current Wildland Fire Patterns and Challenges in Europe: A Synthesis of National Perspectives, Air, Soil and Water Research, https://doi.org/10.1177/11786221211028185, 2021.

Finney, M., Cohen, J., McAllister, S., and Jolly, W.: On the need for a theory of wildland fire spread, International Journal of Wildland Fire, 22, 25, https://doi.org/10.1071/WF11117, 2013.

Forkel, M., Schmidt, L., Zotta, R., Dorigo, W., and Yebra, M.: Estimating leaf moisture content at global scale from passive microwave satellite observations of vegetation optical depth, Hydrology and earth System Sciences, 27, 39–68, https://doi.org/10.5194/hess-27-39-2023, 2023a.

Forkel, M., Schmidt, L., Zotta, R.-M., Dorigo, W., and Yebra, M.: Estimating leaf moisture content at global scale from passive microwave satellite observations of vegetation optical depth, Hydrology and Earth System Sciences, 27, 39–68, https://doi.org/10.5194/hess-27-39-2023, 2023b.

https://doi.org/10.5194/egusphere-2026-1247
Preprint. Discussion started: 16 April 2026

Gibelin, A.-L., Calvet, J.-C., Roujean, J.-L., Jarlan, L., and Los, S.: Ability of the land surface model ISBA-A-gs to simulate leaf area index at the global scale: Comparison with satellites products, Journal of Geophysical Research: Atmospheres, 111, https://doi.org/10.1029/2005JD006691, 2006.

Gupta, H. and Kling, H.: On typical range, sensitivity, and normalization of mean squared error and Nash-Sutcliffe efficiency type metrics, Water Resources Research, 47, 10 601, https://doi.org/10.1029/2011WR010962, 2011.

Jain, P., Coogan, S., Subramanian Sriram, G., Crowley, M., Taylor, S., and Flannigan, M.: A review of machine learning applications in wildfire science management, Environmental Reviews, 28, 478–505, https://doi.org/10.1139/er-2020-0019, 2020.

Jolly, W. and Johnson, D.: Pyro-Ecophysiology: shifting the paradigm of Live Wildland Fuel Research, Fire, 1, 8, https://doi.org/10.3390/fire1010008, 2018.

Jolly, W., Hadlow, A., and Huguet, K.: De-coupling seasonal changes in water content and dry matter to predict live conifer foliar moisture content, International Journal of Wildland Fire, 23, 480, https://doi.org/10.1071/WF13127, 2014.

Kang, Z., Quan, X., and Lai, G.: Assessing the Effects of Fuel Moisture Content on the 2018 Megafires in California, IEEE Journal of Selected Topics in Applied Earth Observations and Remote Sensing, 1, 868–877, https://doi.org/10.1109/JSTARS.2022.3232665, 2023.

Kelley, D., Bistinas, I., Whitley, R., and et al.: How contemporary bioclimatic and human controls change global fire regimes, Nat. Clim. Chang., 9, 690–696, https://doi.org/10.1038/s41558-019-0540-7, 2019.

Kingma, D. P. and Ba, J.: Adam: A Method for Stochastic Optimization, https://arxiv.org/abs/1412.6980, 2017.

Kiranyaz, S., Avci, O., Abdeljaber, O., Ince, T., Gabbouj, M., and Inman, D. J.: 1D convolutional neural networks and applications: A survey, Mechanical Systems and Signal Processing, 151, 107 398, https://doi.org/https://doi.org/10.1016/j.ymssp.2020.107398, 2021.

Liu, X., Martin-StPaul, N., Ruffault, J., Lai, G., Raynal, K., Raquel, R., Wang, H., Parsons, R., Dupuy, J.-L., and Pimont, F.: Drought indices predict changes in live fuel moisture content (LFMC) across French Mediterranean shrublands: a multisource and machine learning approach, Agricultural and Forest Meteorology, 2026.

Loidi, J. and Marcenò, C.: The temperate Deciduous Forests of the Northern Hemisphere. A review, Mediterranean Botany, 43, https://doi.org/10.5209/mbot.75527, 2022.

Luo, K., Quan, X., He, B., and Yebra, M.: Effects of Live Fuel Moisture Content on wildfire occurrence in fire-prone regions over southwest China, Forests, 10, 887, https://doi.org/10.3390/f10100887, 2019.

Martin-StPaul, N., Pimont, F., Dupuy, J., and et al.: Live fuel moisture content (LFMC) time series for multiple sites and species in the French Mediterranean area since 1996, Annals of Forest Science, 75, 57, https://doi.org/10.1007/s13595-018-0729-3, 2018.

Masson, V., Le Moigne, P., Martin, E., Faroux, S., Alias, A., Alkama, R., Belamari, S., Barbu, A., Boone, A., Bouyssel, F., and et al.: The SURFEXv7.2 Land and Ocean Surface Platform for Coupled or Offline Simulation of Earth Surface Variables and Fluxes, Geoscientific Model Development, 6, https://doi.org/10.5194/gmd-6-929-2013, 2013.

McCaffrey, S.: Thinking of Wildfire as a Natural Hazard, Society & Natural Resources, 17, 509–516, https://doi.org/10.1080/08941920490452445, 2004.

McNorton, J. and Di Giuseppe, F.: A global fuel characteristic model and dataset for wildfire prediction, Biogeosciences, 21, 279–300, https://doi.org/10.5194/bg-21-279-2024, 2024.

Miller, C. and Ager, A.: A review of recent advances in risk analysis for wildfire management, International Journal of Wildland Fire, 22, 1–14, https://doi.org/10.1071/WF11114, 2012.

https://doi.org/10.5194/egusphere-2026-1247
Preprint. Discussion started: 16 April 2026

Moesinger, L., Dorigo, W., de Jeu, R., van der Schalie, R., Scanlon, T., Teubner, I., and Forkel, M.: The global long-term microwave Vegetation Optical Depth Climate Archive (VODCA), Earth System Science Data, pp. 177–196, https://doi.org/10.5194/essd-12-177-2020, 2020.

Nash, J. and Sutcliffe, J.: River flow forecasting through conceptual models part I — A discussion of principles, Journal of Hydrology, 10, 282–290, https://doi.org/10.1016/0022-1694(70)90255-6, 1970.

Noilhan, J. and Planton, S.: A Simple Parameterization of Land Surface Processes for Meteorological Models, Monthly Weather Review, 117, https://doi.org/10.1175/1520-0493(1989)117<0536:ASPOLS>2.0.CO;2, 1989.

Pimont, F., Ruffault, D., Martin-StPaul, N., and Dupuy, J.: Why is the Effect of LFMC on Fire Rate of Spread Underestimated in Field Experiments in Shrublands?, International Journal of Wildland Fire, 28, 127–137, https://doi.org/10.1071/WF18091, 2019.

Pimont, F., Ruffault, J., Opitz, T., Fargeon, H., Barbero, R., and et al.: Future expansion, seasonal lengthening and intensification of fire activity under climate change in southeastern France, International Journal of Wildland Fire, 32, 4–14, https://doi.org/10.1071/WF22103, 2023.

Preisler, H., Brillinger, D., Burgan, R., and Benoit, J.: Probability based models for estimation of wildfire risk, International Journal of Wildland Fire, 13, 133, https://doi.org/10.1071/wf02061, 2004.

Rao, K., Williams, A., Fortin Flefil, F., and Konings, A.: SAR-enhanced mapping of live fuel moisture content, Remote Sensing of Environment, 245, https://doi.org/10.1016/j.rse.2020.111797, 2020.

Rodriguez-Jiménez, F., Lorenzo, H., Novo, A., C., A.-A., and Alvarez, X.: Modelling of live fuel moisture content in different vegetation scenarios during dry periods using meteorological data and spectral indices, Forest Ecology and Management, 546, 121 378, https://doi.org/10.1016/j.foreco.2023.121378, 2023.

Rojas-Munoz, O., Calvet, J.-C., Bonan, B., Baghdadi, N., Meurey, C., Napoly, A., Wigneron, J.-P., and Zribi, M.: Soil Moisture Monitoring at Kilometer Scale: Assimilation of Sentinel-1 Products in ISBA, Remote Sensing, 15, https://doi.org/10.3390/rs15174329, 2023.

Rothermel, R.: A mathematical model for predicting fire spread in wildland fuels, Department of Agriculture, Intermountain Forest and Range Experiment Station, https://research.fs.usda.gov/treesearch/32533, 1972.

Seity, Y., Brousseau, P., Malardel, S., Hello, G., Bénard, P., Bouttier, F., Lac, C., and Masson, V.: The AROME-France Convective-Scale Operational Model, Monthly Weather Review, 139, 976 – 991, https://doi.org/10.1175/2010MWR3425.1, 2011.

Shams Eddin, M. H., Roscher, R., and Gall, J.: Location-Aware Adaptive Normalization: A Deep Learning Approach for Wildfire Danger Forecasting, IEEE Transactions on Geoscience and Remote Sensing, 61, 1–18, https://doi.org/10.1109/TGRS.2023.3285401, 2023.

Skinner, R., Luther, M., Hertelendy, A., Khorram-Manesh, A., Sørensen, J., Goniewicz, K., and Ranse, J.: A Literature Review on the Impact of Wildfires on Emergency Departments: Enhancing Disaster Preparedness, Prehosp Disaster Med, 37, 657–664, https://doi.org/10.1017/S1049023X22001054, 2022.

Viñuales, A., Montes, F., Guijarro, M., Gómez, C., De la Calle, I., and Madrigal, J.: Real-time assessment of live forest fuel moisture content and flammability by using space-time universal kriging, Ecological Modelling, 498, 110 867, https://doi.org/10.1016/j.ecolmodel.2024.110867, 2024.

Wang, X., Wotton, B. M., Cantin, A. S., Parisien, M.-A., Anderson, K., Moore, B., and Flannigan, M. D.: cffdrs: an R package for the Canadian Forest Fire Danger Rating System, Ecological Processes, https://doi.org/10.1186/s13717-017-0070-z, 2017.

Yebra, M., Scortechini, G., Adeline, K., and et al.: Globe-LFMC 2.0, an enhanced and updated dataset for live fuel moisture content research, Scientific Data, 11, 332, https://doi.org/10.1038/s41597-024-03159-6, 2024.